JOURNAL OF THERMOPHYSICS AND HEAT TRANSFER
Vol. 21, No. 2, April–June 2007

Heat Transfer from Protuberances

Stephen T. McClain*
University of Alabama at Birmingham, Birmingham, Alabama 35294-4461
Mario Vargas† and Richard E. Kreeger†
NASA John H. Glenn Research Center at Lewis Field, Cleveland, Ohio 44135
and
Jen-Ching Tsao‡
Ohio Aerospace Institute, Cleveland, Ohio 44135

DOI: 10.2514/1.23186

An experiment by Henry et al. (Henry, R. C., Hansman, R. J., Breuer, K. S., "Heat Transfer Variation on Protuberances and Surface Roughness Elements," *Journal of Thermophysics and Heat Transfer*, Vol. 91, Mar. 1995, pp. 175–180.) explored the heat transfer of flows over protuberances in laminar and turbulent flow, simulating conditions during the beginning stages of glaze icing. This paper represents an effort to explain the heat transfer enhancement of roughness elements and protuberances that was observed by Henry et al. In the experiments of Henry et al., a single roughness element was placed on a heated flat plate. The temperature along the flat plate and along the roughness element was measured using an infrared camera to determine the enhancement of heat transfer of the protuberance as opposed to the smooth surface. A one-dimensional extended-surface (fin) analysis was performed to examine the results of Henry et al. Although significant assumptions were made using the extended-surface analysis, the important trends of the Henry et al. data were captured. The extended-surface analysis captured the trends of the apparent enhancement as reported by Henry et al. vs the Reynolds number based on the location from the leading edge of the surface and vs the ratio of the protuberance height to the boundary-layer thickness. Although the absolute magnitudes of the apparent enhancement are overestimated by the extended-surface analysis, the matched trends indicate the importance of the thermal conductivity of the protuberance, the importance of the interaction of the protuberance with the thermal boundary layer, and the importance of radiation into the protuberance.

Nomenclature

A	=	area
d	=	diameter
h	=	heat transfer coefficient
k	=	roughness element height
k_f	=	fluid thermal conductivity
k_R	=	roughness element thermal conductivity
Nu	=	Nusselt number
Pr	=	Prandtl number
Q	=	heat rate
q''	=	heat flux per unit area
Re	=	Reynolds number
T	=	temperature
u	=	streamwise velocity
v	=	wall-normal velocity
x	=	streamwise direction
y	=	wall-normal direction
θ	=	normalized temperature

Subscripts

c	=	convection
cd	=	conduction
D	=	drag
d	=	diameter
f	=	fluid or fin
p	=	perturbed
R	=	roughness element
r	=	radiation
s	=	surface
u	=	unperturbed
w	=	wall
0	=	value at base of protuberance
∞	=	freestream

Presented as Paper 1082 at the 44th AIAA Aerospace Sciences Meeting and Exhibit, Reno, NV, 9–12 January 2006; received 13 February 2006; revision received 19 July 2006; accepted for publication 2 September 2006.

*Assistant Professor, Department of Mechanical Engineering, 1530 Third Avenue South, BEC Building, Room 358B. AIAA Member.
†Aerospace Engineer, Icing Research Branch, Mail Stop 11-2. Member AIAA.
‡Senior Scientist, Icing Research Branch, Mail Stop 11-2. Senior Member AIAA.

I. Introduction

ICE accretion formation on swept wings is characterized by the presence of icing structures known as scallops or lobster tails. Those structures are made primarily of icing feathers that have grown from roughness elements of a height comparable with or larger than the boundary layer at the element location [1]. The growth of the elements into feathers is related to the heat transfer from the complex interaction between the element, the freestream flowfield, and the boundary-layer development. The modeling and prediction of local and bulk surface heat transfer over the type of roughness elements encountered in icing is needed for the development of models of ice accretion formation on swept wings that can be incorporated into 3-D ice accretion codes.

Past icing-related studies on the effect of large roughness elements on boundary-layer development, flowfield, and heat transfer at the Mach numbers encountered in icing were conducted on flat plates and unswept airfoils. No work has been conducted on swept wings, but the work on flat plates and unswept airfoils is considered a first step in that direction because it allows the development of analytical, experimental, and computational techniques in simpler configurations before the techniques are extended to a swept wing configuration.

Initial measurements of the local variation of heat transfer over roughness elements were conducted by Henry et al. [2] using infrared (IR) measurement techniques. For laminar and turbulent boundary layers, they measured heat transfer enhancement (the ratio of the

local heat transfer coefficient over a roughness element to the heat transfer coefficient at a location without roughness elements) over single isolated roughness elements or protuberances. They observed heat transfer enhancement over the roughness element, with the maximum value occurring on the upstream face. The heat transfer enhancement was observed to increase as the height of the element increased with respect to the boundary-layer thickness. For the turbulent boundary-layer case, they also measured the heat transfer enhancement over multiple roughness elements and studied the effect of element spacing.

Lee [3] conducted heat transfer measurements by implementing the setup of Henry et al. [2] on a NACA 0012 unswept airfoil with distributed roughness. The configuration was the same that Kerho [4] used to study the effect of distributed roughness on the development of an airfoil boundary layer on an unswept NACA 0012. Because Lee's setup was the same as Kerho's, he could relate the heat transfer results to the state of the boundary layer. Like Henry et al., Lee measured the heat transfer enhancement: the ratio of the heat transfer coefficient in the perturbed region to the heat transfer coefficient in a region of unperturbed laminar boundary layer at the same chordwise distance. For the leading edge roughness case, he observed that the heat transfer rates over and immediately downstream of the roughness were higher than the turbulent smooth-wall values. Increasing the Reynolds number increased the heat transfer enhancement over and downstream of the roughness. Increasing freestream turbulence had no significant effect on heat transfer enhancement due to the leading edge roughness.

Several researchers have conducted nonlocal measurements (average over a given area) of heat transfer coefficients over surfaces with roughness of the type encountered in ice accretions. Dukhan [5] measured heat transfer coefficients over eight test strips outfitted with flux gauges. The test strips were taken from aluminum castings of ice accretion shapes grown on flat plates in the NASA Glenn Icing Research Tunnel. They found that, beyond a certain level of roughness, there was no change in the heat transfer coefficient. Poinsatte [6] measured the heat transfer coefficient over a NACA 0012 airfoil with and without artificial roughness for Reynolds numbers in the range of 1.24×10^6 to 2.50×10^6. The roughness was simulated by attaching 2-mm-diam hemispheres to the airfoil in four different patterns. He observed that the presence of roughness produced a large increase in the heat transfer compared with the smooth airfoil case. He also observed that the heat transfer coefficient increased when the number of roughness elements in a given area increased (dense pattern) and when the angle of attack was increased.

Because the Henry et al. [2] experiment is the only local measurement of heat enhancement over single roughness elements, their data is critical in the validation of current computational fluid dynamics (CFD) simulations [7] of heat transfer over roughness elements of the size encountered in icing. In addition, the experiment is the starting point of further experimental studies being planned to obtain data to model ice accretions on swept wings. For those reasons, it is important to reexamine the methodology and assumptions used in the Henry et al. experiment to gain understanding for the design of future experimental work and for the modeling of heat transfer over roughness elements.

This paper presents the development of a one-dimensional extended-surface (fin) analysis to calculate the heat transfer over single roughness elements and its application to the Henry et al. [2] experiment. The present work is the first part of the development of an extended-surface, discrete-element methodology (ES-DEM) for the calculation of heat transfer over large roughness elements.

II. Background Information

In the Henry et al. [2] experiments, a single spherical-segment protuberance, made of plastic, was placed on a flat plate heated using infrared lamps. The temperature along the flat plate and along the protuberance was measured using an infrared camera to determine the enhancement of heat transfer of the protuberance as opposed to the smooth surface. Figure 1 demonstrates how the protuberances were placed on a Plexiglas plate, 0.25 m from the leading edge.

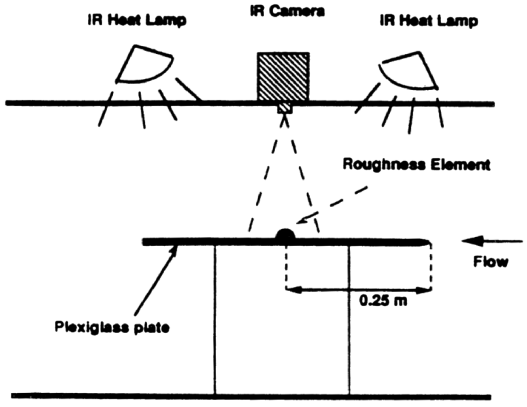

Fig. 1 The experimental system of Henry et al. [2] (reprinted with permission of the authors).

The infrared camera was used to make measurements of the temperature along the flat Plexiglas surface and along the surface of the protuberance. The temperatures were then used to determine the heat transfer enhancement. In the development of the local heat transfer enhancement, Henry et al. [2] assumed that the conduction into the Plexiglas plate was negligible and that the heat that entered the surface from the infrared heat lamps was completely dissipated from the surface by convection. If, on each part of the surface, the convection heat transfer equals the radiation heat transfer and the radiation heat transfer into the surface does not vary along the surface, then Henry et al. reasoned that

$$q_r'' = q_c'' = h_u(T_u - T_\infty) = h_p(T_p - T_\infty) \tag{1}$$

Defining the heat transfer enhancement as the ratio of the convection coefficient on the protuberance over the convection coefficient on the unperturbed surface at the same distance from the leading edge, the heat transfer enhancement was evaluated as

$$\frac{h_p}{h_u} = \frac{T_u - T_\infty}{T_p - T_\infty} \tag{2}$$

As described by Eq. (2), the local heat transfer enhancement is the ratio of the temperature difference on the unperturbed surface to the freestream temperature divided by the temperature difference on the protuberance surface to the freestream temperature. Henry et al. [2] used an infrared camera with a reported pixel resolution of 1 mm to measure the temperature on the surface of each protuberance and the region surrounding the protuberance. Figure 2 presents the local heat transfer enhancement, as determined using Eq. (2) and the local temperature measurements, for the 2.8-mm-tall protuberance for laminar flow.

Figure 2 shows how the heat transfer enhancement along the element and behind the element increased as the freestream velocity increased in laminar flow. Figure 3 presents the enhancement for the same protuberance turbulent flow. Figures 2 and 3 show two

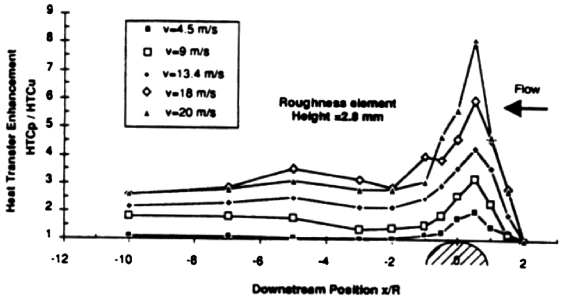

Fig. 2 Heat transfer enhancement on the 2.8-mm protuberance in laminar flow at various freestream velocities (from Henry et al. [2], reprinted with permission of the authors).

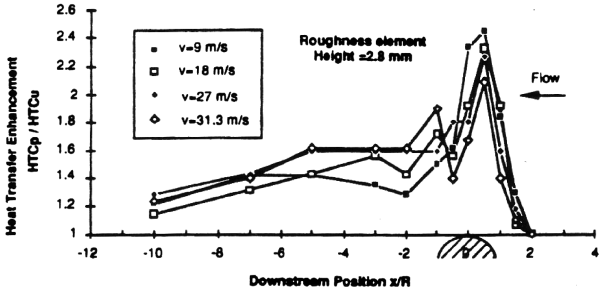

Fig. 3 Heat transfer enhancement on the 2.8-mm protuberance in turbulent flow at various freestream velocities (from Henry et al. [2], reprinted with permission of the authors).

important secondary flow features. The maximum local heat transfer enhancement (minimum local temperature) occurred on the upstream face of the protuberances just before the apex of the protuberances. For the higher flow rates in laminar flow, the enhancement did not approach a value of 1.0 behind the protuberance. The elevated values of enhancement behind the protuberances at high speeds demonstrated that the flow had separated and was causing higher transitional heat transfer rates behind the protuberances.

Another important contribution of Henry et al. [2] was the identification of the maximum enhancement for each protuberance as a function of Reynolds number based on location from the leading edge of the plate, presented in Fig. 4, and vs the ratio of the protuberance height over the boundary-layer thickness, presented in Fig. 5. Figure 4 shows that as the Reynolds number increased in laminar flow, the heat transfer enhancement increased until the flow naturally transitioned to turbulent flow. Once transition began, the heat transfer enhancement decreased. Figure 5 presents the heat transfer enhancement vs the ratio of the protuberance height over the unperturbed boundary-layer thickness for all four protuberance sizes. Figure 5 suggests that the heat transfer enhancement increases

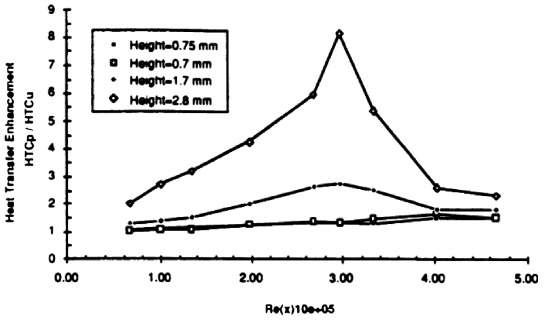

Fig. 4 The heat transfer enhancement in laminar and naturally transitioning flow vs Reynolds number based on the distance of the protuberances from the leading edge of the Plexiglas plate (Fig. 7 of Henry et al. [2], reprinted with permission of the authors).

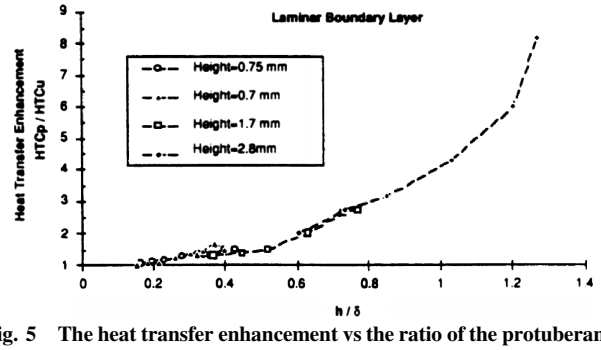

Fig. 5 The heat transfer enhancement vs the ratio of the protuberance height over the boundary-layer thickness in laminar flow (Fig. 8 of Henry et al. [2], reprinted with permission of the authors).

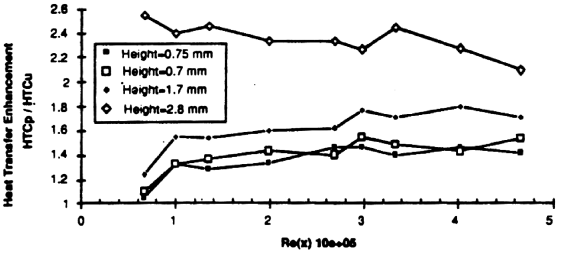

Fig. 6 The heat transfer enhancement in turbulent flow vs Reynolds number based on the distance of the protuberances from the leading edge of the Plexiglas plate (Fig. 11 of Henry et al. [2], reprinted with permission of the authors).

exponentially with increasing protuberance height above the boundary-layer thickness.

Henry et al. [2] also made measurements of the heat transfer enhancement of protuberances in flow that had been artificially tripped to turbulent flow at the leading edge of the Plexiglas plate. Figure 6 presents the reported enhancement of the protuberances in turbulent flow as a function of Reynolds number from the leading edge of the plate. As for the laminar flow cases, Henry et al. found that the maximum enhancement (lowest local protuberance temperature) occurs just upstream of the apex of the spherical-segment protuberance (Fig. 3).

Although their findings were enlightening, Henry et al. [2] noted several interesting results:

1) For both laminar and turbulent flow, the maximum enhancement occurred before the apex of the protuberances.

2) The large protuberances produced a significant enhancement downstream of the protuberances, indicating separation of the flow from the protuberance.

3) The values of enhancement measured for the laminar cases were much greater than the cases for turbulent flow for the largest protuberance.

4) The heat transfer enhancement increased exponentially with respect to the ratio of protuberance height over boundary-layer thickness.

5) The enhancement decreased with Reynolds number for the largest protuberance in turbulent flow.

Because of the expected dependence of feather growth and formation on local roughness element heat transfer, the objectives of this effort were to 1) develop a better understanding of the physics involved in the experimental situations described by Henry et al. [2] and the causes of the findings and 2) develop a model to predict the heat transfer from protuberances in laminar and turbulent flow.

III. Extended-Surface Analysis

In the experiments of Henry et al. [2], the temperature changes along the height of the protuberances because they are *extended surfaces* (fins). To predict the temperature changes along the height of the protuberances, an extended-surface equation was developed that included the radiation into protuberance and local convection coefficient at each height. Figure 7 depicts the physical situation and the control volume used to develop the extended-surface equation.

When the extended-surface equation is derived with the assumed heat transfer directions shown in Fig. 7, the result is

$$\frac{d^2T_R}{dy^2} + \frac{1}{A}\frac{dA}{dy}\frac{dT_R}{dy} - \frac{h_d(T_R - T_f)}{k_R A}\frac{dA_s}{dy} - \frac{q_r''}{k_R A}\frac{dA_s}{dy} = 0 \qquad (3a)$$

with boundary conditions of 1) at the wall, the temperature of the roughness element equals the temperature of the wall and 2) the heat conducted through the base of the element must equal the heat convected and radiated from the extended surface of the roughness element.

$$T_R(0) = T_w \qquad (3b)$$

and

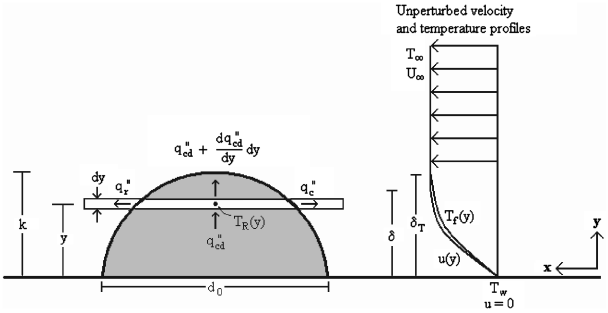

Fig. 7 Protuberance control volume for extended-surface analysis.

$$k_R A \left.\frac{dT_R}{dy}\right|_{y=0} = \int_0^k \left[h_d \frac{dA_s}{dy}(T_R - T_f) + q''_r \frac{dA_s}{dy} \right] dy \qquad (3c)$$

In Eq. (3a), A is the planform cross-sectional area of the protuberance at a given height y, and A_s is the wetted convection area at a given height y. Equation (3) may be partly normalized using the variable transformations:

$$\theta_R = \frac{T_R - T_\infty}{T_w - T_\infty} \quad \text{and} \quad \theta_f = \frac{T_f - T_\infty}{T_w - T_\infty}$$

yielding

$$\frac{d^2\theta_R}{dy^2} + \frac{1}{A}\frac{dA}{dy}\frac{d\theta_R}{dy} - \frac{1}{k_R A}\frac{dA_s}{dy}\left[h_d(\theta_R - \theta_f) + \frac{q''_r}{T_w - T_\infty} \right] = 0 \qquad (4a)$$

with the boundary conditions

$$\theta_R(0) = 1 \qquad (4b)$$

and

$$\left.\frac{d\theta_R}{dy}\right|_{y=0} = \frac{\int_0^k [h_d \frac{dA_s}{dy}(\theta_R - \theta_f) + \frac{q''_r}{T_w - T_\infty}\frac{dA_s}{dy}]\, dy}{A_0 k_R} \qquad (4c)$$

The fact that the radiation term is not normalized will be discussed in a following section.

Numerical solution of Eq. (4a) requires a "shooting" technique. The temperature gradient at the wall must be guessed, which implies a conduction heat flux through the base of the element. Equation (4a) is then integrated, and the heat convected and radiated out of the extended surface is calculated using the right-hand side of Eq. (4c). If the calculated flux from the extended surface does not equal the guessed conduction heat flux through the base, a new guess is calculated for the next iteration. The resulting temperature profiles are highly sensitive to the initial guess of the temperature gradient at the base, and relaxation values of around 0.01 are required for converged numerical solutions. Because the relaxation values are so low, numerical solution of Eq. (4a) can require significant computational time.

A. Fluid Velocity and Temperature Profile Evaluation

For flows over a protuberance, the velocity and temperature profiles are not easily evaluated without the use of CFD codes. The local fluid velocity and temperature are required to determine the local convective flux from the protuberance to the fluid. For the extended-surface analysis, the velocity and temperature profiles impinging the protuberance were assumed to be the same as the unperturbed velocity and temperature profiles. This assumption seems reasonable, based on the fact that for flow over a protuberance, the fluid does not have significant time or space to adjust to the decreased flow volume, increased drag, and altered heat transfer, compared with the unperturbed flow.

Different methods to determine the velocity and temperature profiles were used for laminar and turbulent flows. In the following subsections, the different methods for determining the velocity and temperature profiles are described.

1. *Laminar Flows*

For laminar flows over a flat plate with a constant heat flux and zero flow acceleration, the boundary-layer equations can be reduced to two coupled differential equations [8]. The coupled differential equations were solved using MathCAD's fourth-order Runge–Kutta solver.

2. *Turbulent Flows*

For the turbulent cases, BLACOMP was used to generate the velocity and temperature profiles. BLACOMP is a two-dimensional finite difference boundary-layer solver that was generated at Mississippi State University for educational purposes. BLACOMP has been validated for many two-dimensional flat plate configurations [9]. In developing the unperturbed profiles, the Prandtl mixing length model with van Driest damping and $Pr_t = 0.9$ was used for turbulent closure.

B. Local Protuberance Convection Coefficient

To calculate the local convective heat transfer coefficient h_d in Eq. (4c), correlations from the discrete-element model were used. The discrete-element model is an engineering tool for predicting skin friction and heat transfer for turbulent flows over surfaces with distributed roughness. The model is formulated for roughness elements with three-dimensional shapes for which the element cross section can be defined at every height y in turbulent flow [10]. The differential equations, including roughness effects, are derived by applying the basic conservation statements for mass, momentum, and energy to a control volume, such as that shown in Fig. 8. Basic to this approach is the idea that the two-dimensional, time-averaged turbulent boundary-layer equations can be applied in the flow region below the crests of the roughness elements. The flow variables are spatially averaged over the transverse z direction and the streamwise x direction. The physical effects of the roughness elements on the fluid in the control volume are modeled by considering the flow blockage, the local element heat transfer, and the local element form drag.

In the discrete-element model, the form drag force on the control volume is due to the portion of the roughness elements penetrating the control volume and is expressed using a local drag coefficient. Likewise, the rate of heat transfer between the portion of the roughness elements penetrating the control volume and the fluid is expressed using a local Nusselt number as

$$Q = \pi k_f (T_R - T)\delta y N u_d \qquad (5)$$

Nu_d is formulated as functions of the local roughness element Reynolds number:

$$Re_d = \frac{\rho u d}{\mu} \qquad (6)$$

where u and d are functions of the distance from the wall. Thus, the discrete-element model directly includes information on the roughness element size and shape. The functional form for Nu_d used

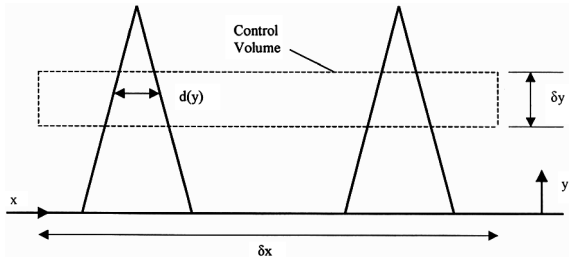

Fig. 8 The discrete-element roughness model control volume schematic.

in this study for circular roughness elements is [10]

$$Nu_d = \begin{cases} 1.7Re_d^{0.49}Pr^{0.4} & \text{for } Re_d \le 13,776 \\ 0.0605Re_d^{0.84}Pr^{0.4} & \text{for } Re_d > 13,776 \end{cases} \quad (7)$$

The functional form Nu_d was constructed by beginning with the heat transfer relationships for banks of cylinders in crossflow, followed by extensive calibrations using a number of deterministic surface roughness data sets. Based on the local Nusselt number, the local convection coefficient is then

$$h_d = \frac{k_f Nu_d}{d} \quad (8)$$

Although the physical phenomena of Henry et al. [2] is for a single protuberance in laminar and turbulent flow with no wake interaction with other roughness elements, the relationship provided by the discrete-element model for turbulent flow over distributed roughness elements is an alternative for evaluating local element heat transfer.

C. Radiation into the Protuberance

In Eq. (4a), the radiation term was not normalized, because of its independence of the temperature difference between the fluid and the protuberance surface. The radiation is dependent on the temperature of the wall, or protuberance surface, and the temperature of the radiant heat lamps used in the study. Had the radiant heat input been the same for each case run by Henry et al. [2], solving the extended-surface equation would have been difficult, because Henry et al. did not report the unperturbed surface temperature for each case they observed.

From their reported observations of the unperturbed surface temperatures, however, it is clear that the radiation input to the surface was not constant between runs. Henry et al. [2] report that for their low-speed, laminar cases (5 m/s), the typical unperturbed temperature difference between the wall and the freestream was around 17 K. Henry et al. also report that for a high-speed, turbulent case (31.3 m/s), the typical unperturbed temperature difference between the wall and the freestream was approximately 9 K.

In the unperturbed regions, the assumption of negligible conduction through the Plexiglas plate is reasonable. Thus, in the unperturbed regions, the heat convected from the plate to the freestream must equal the radiation input from the heat lamps to the plate. The Nusselt number for laminar flow with constant heat flux and $0.5 < Pr < 10$ is [8]

$$Nu_x = \frac{q_c''}{T_w - T_\infty}\frac{x}{k_f} = 0.453Re_x^{1/2}Pr^{1/3} \quad (9)$$

Thus, for the low-speed laminar case reported by Henry et al. [2], the apparent radiation heat flux in the unperturbed region at the same distance from the leading edge of the Plexiglas plate is

$$q_r'' = q_c'' = (T_w - T_\infty)\frac{k_f}{x}0.453Re_x^{1/2}Pr^{1/3} \cong 200\frac{W}{m^2}$$

The Nusselt number for turbulent flow with constant heat flux is [8]

$$Nu_x = \frac{q_c''}{T_w - T_\infty}\frac{x}{k_f} = 0.0296Re_x^{4/5}Pr^{1/3} \quad (10)$$

(Note: Eq. (16) is the local Nusselt expression for turbulent flow over a flat plate with uniform temperature. Bejan [8] reports that using Eq. (16) for the uniform flux case is satisfactory and the error involved in doing so is less than 4%.) For the high-speed, turbulent case reported by Henry et al. [2], the apparent radiation heat flux in the unperturbed region is then

$$q_r'' = q_c'' = (T_w - T_\infty)\frac{k_f}{x}0.0296Re_x^{4/5}Pr^{1/3} \cong 900\frac{W}{m^2}$$

Thus, the radiant flux into the flat plate is considerably different for the two example cases discussed by Henry et al. [2]. In the sense that Eq. (4) cannot be normalized with a constant radiation, the complication that the radiation is not the same from case to case is surmountable.

Because the radiation flux into the surface is assumed to equal the convected flux in the unperturbed region, an alternative exists for evaluating the radiation heat flux into the protuberance. If it is assumed that the radiative heat flux into the protuberance equals the radiative heat flux into the unperturbed region, then

$$q_r'' = q_{c,\text{unp}}'' = h_x(T_w - T_\infty) \quad (11)$$

The radiation term in Eq. (4a) is then

$$\frac{q_r''}{(T_w - T_\infty)} = h_x = \frac{k_f}{x}Nu_x \quad (12)$$

where Nu_x is evaluated using Eq. (9) for laminar flow or Eq. (10) for turbulent flow. Using Eqs. (9) or (10) to evaluate the radiative heat flux, Eq. (4a) is normalized in that it is independent of the magnitudes of T_w, T_∞, or T_w-T_∞. The final normalized form of Eq. (4a) is

$$\frac{\mathrm{d}^2\theta_R}{\mathrm{d}y^2} + \frac{1}{A}\frac{\mathrm{d}A}{\mathrm{d}y}\frac{\mathrm{d}\theta_R}{\mathrm{d}y} - \frac{1}{kA}\frac{\mathrm{d}A_s}{\mathrm{d}y}[h_d(\theta_R - \theta_f) + h_x] = 0 \quad (13)$$

The boundary conditions for the extended-surface equation are not changed.

D. List of Important Assumptions in Extended-Surface Analysis

Many assumptions are made in the extended-surface, discrete-element (ES-DEM) analysis to *model* the convection from the roughness element to the fluid, the internal conduction in the protuberance, and the radiation into the protuberance. The assumptions believed to have the largest impact on the predictions of protuberance temperature in the ES-DEM analysis are as follows:

1) The velocity and temperature profiles impinging the protuberance are the same as the unperturbed velocity and temperature profiles.

2) The flow around the protuberance at any height y is parallel to the wall and behaves as a two-dimensional flow (in the x–z plane) around a cylinder with the diameter of the protuberance at the given height.

3) The local protuberance convection coefficient h_d is an average value around the circumference of the protuberance at a given elevation.

4) The temperature of the protuberance is constant around its circumference at a given elevation.

5) Radial internal conduction resistance in the protuberance is negligible.

6) The temperature of the wall surrounding the protuberance is not affected by the presence of the protuberance; that is, the temperature of the wall at the base of the protuberance equals the temperature of the wall in the unperturbed region at the same distance from the leading edge of the plate.

7) The radiative heat flux on the surface of the protuberance is constant over the surface of the protuberance and equals the convective heat flux on the unperturbed region of the wall at the same distance from the leading edge of the plate as the protuberance.

8) The Plexiglas plate receives a constant radiative flux along the direction of the flow, implying that Eqs. (15) and (16) are appropriate for determining the local unperturbed wall flux at the distance of the protuberance from the leading edge of the plate.

Although many assumptions are made, recall that modeling efforts take complex physical phenomena and assume that some variables are more or less important than others. The intent of modeling efforts is to obtain order of magnitude estimates and capture trends of experimental measurements. When trends are not captured, variables that were assumed to have a secondary influence or other previously neglected variables are having primary influences on the measured phenomena.

Many variables that were assumed negligible in the ES-DEM analysis are suspected of affecting ice accretion features such as horns, feathers, and scallops. Further investigation of these

secondary features is required. However, creating a simulation to evaluate the appropriateness of *all* of the assumptions is not practical with current computational technology. Assumptions 1, 2, and 3 will be evaluated in the near future using CFD simulations. Evaluating assumptions 4, 5, and 6 would require a complete conjugate analysis, a coupled CFD analysis of the fluid, and a finite-element analysis of the heat transfer in the protuberance. Evaluating assumptions 7 and 8 will require more information regarding surface temperatures than was reported by Henry et al. [2] and a complex radiation analysis.

The assumptions listed previously were assumptions regarding the fluid and thermal physics. There is another assumption made regarding a material property that significantly affects the ES-DEM analysis. This assumption is the value of the thermal conductivity of the protuberance material. The thermal conductivity of the protuberance material is not easily evaluated. Henry et al. [2] report that the protuberances were constructed using "plastic hemispherical beads." However, Henry et al. did not specify what type of plastic, and different types of plastic can have significantly different thermal conductivities. Further complicating the issue, reported values for the thermal conductivity of plastic varied from 0.15 $\mathrm{W/m \cdot K}$ to 0.35 $\mathrm{W/m \cdot K}$. The value used in the ES-DEM analyses was 0.19 $\mathrm{W/m \cdot K}$, as reported by Kreith [11].

IV. ES-DEM Results and Comparison with Data from Henry et al. [2]

Even with the major assumptions listed, the ES-DEM analysis of the protuberance is enlightening. For five laminar fluid velocities and four turbulent fluid velocities, the temperature profiles in the protuberances were determined using the ES-DEM analysis. The analyses were performed for protuberance heights of $k = 2.8$ and 1.7 mm. The extended-surface, discrete-element methodology can be summarized as follows:

1) The velocity and temperature profiles were determined by integrating the similarity solution (laminar flow) or by a finite difference boundary-layer code (turbulent flow)

2) Using the local fluid velocity information, the discrete-element correlations were used to determine the local protuberance convection coefficients.

3) The fin equation was integrated numerically to evaluate the internal conduction.

A. Laminar Flow Results

Figure 9 shows the ES-DEM predictions of the apparent enhancement, evaluated using the predicted temperatures and Eq. (2), on the 2.8-mm-tall protuberance in laminar flow. Figure 9 is a direct comparison to Fig. 2. Although the apparent enhancement is not a true measure of the change in local heat transfer (as will be shown hereafter), the results are presented in terms of the apparent enhancement for direct comparison to the figures presented by Henry et al. [2]. Figure 9 shows that the ES-DEM overpredicts the apparent enhancement. For the 20 m/s case, for example, the ES-DEM

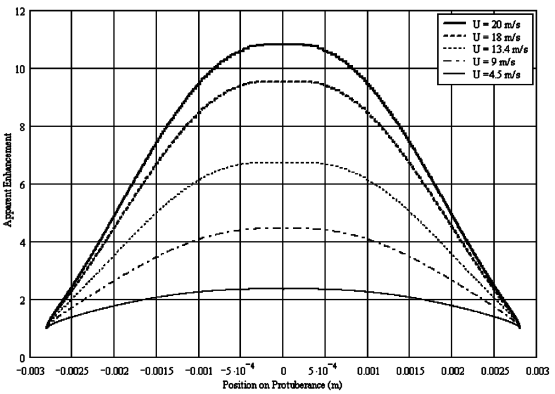

Fig. 9 Prediction of perceived heat transfer enhancement profiles on a 2.8-mm protuberance in laminar flow as a comparison with Fig. 4.

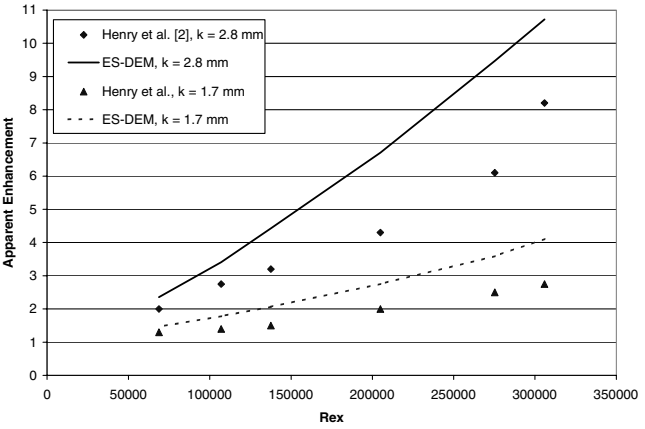

Fig. 10 Apparent maximum heat transfer enhancement in laminar flow vs Reynolds number for comparison with Fig. 4.

predictions of the maximum apparent enhancement is 10.72, whereas Henry et al. measured a maximum apparent enhancement of 8.2. However, the order of magnitude of the apparent enhancement is captured, and the primary objective of the modeling effort is to capture the trends of the Henry et al. data.

Figure 10 displays the apparent enhancement in laminar flow for the 2.8 and 1.7-mm protuberances vs the Reynolds number, based on the distance of the protuberance from the leading edge of the Plexiglas plate. Figure 10 demonstrates that the ES-DEM analysis captures the trends exhibited in the experimental data: that the apparent enhancement increases as the Reynolds number increases for a given protuberance height. Figure 10 is a direct comparison to Fig. 4 for the laminar cases.

Figure 11 presents the apparent enhancement in laminar flow for the 2.8 and 1.7-mm protuberances vs the ratio of the protuberance height over the boundary-layer thickness, as determined using

$$\delta = 4.92 x Re_x^{-0.5} \tag{14}$$

The ES-DEM analysis predicts the trends exhibited by the measured apparent enhancements very well. The measured apparent enhancements and the ES-DEM predictions of the apparent enhancement all increase very rapidly as the protuberances become larger than the boundary-layer thickness (k/δ increases).

Henry et al. [2] explain the trend of increasing apparent enhancement as the Reynolds number and k/δ increase as being "due to increased ventilation experienced by the roughness as it protrudes through the boundary layer." It is true that as the local velocity at a given height on a protuberance increases, the local convection coefficient also increases. This is readily apparent in Eq. (7). Figure 12 shows the local protuberance convection coefficient along

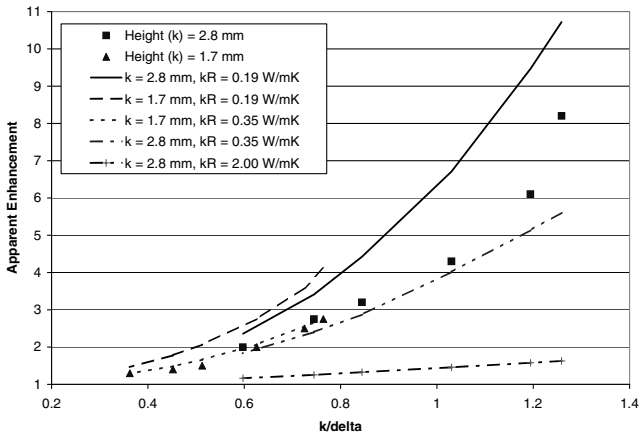

Fig. 11 Apparent heat transfer enhancement vs the ratio of the protuberance height over the undisturbed laminar boundary-layer thickness for comparison with Fig. 5.

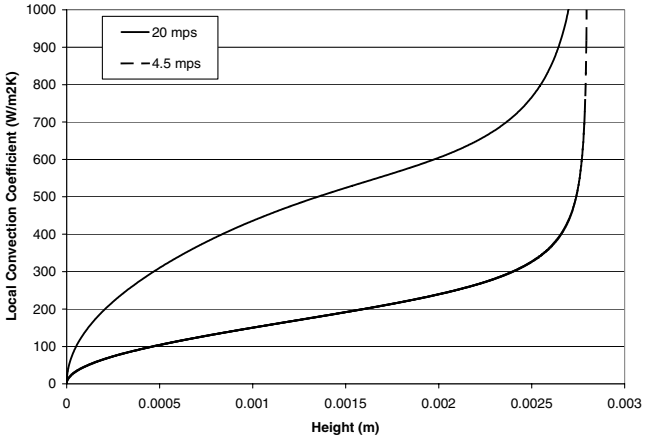

Fig. 12 The local protuberance convection coefficient in laminar flow for freestream velocities of 20 and 4.5 m/s.

the height of the protuberance for freestream velocities of 20 and 4.5 m/s. At the middle elevation of the protuberance, the local convection coefficient for the 20 m/s case is over 2.5 times that for the 4.5 m/s case.

However, the increased convection coefficients are only a part of the explanation. The driving term in Eq. (13) that determines the temperature of the protuberance at a given elevation is

$$h_d(\theta_R - \theta_f) + h_x \tag{15}$$

Each term of Eq. (15) determines the shape of θ_R and contributes to the increased apparent enhancements exhibited by the protuberances.

Figure 13 shows the fluid temperature and the protuberance temperature profiles for freestream velocities of 20 m/s and 4.5 m/s. Because the thermal boundary-layer thickness is much taller for the 4.5 m/s case, the fluid temperature at a given elevation is much warmer than the fluid temperature at the same elevation for the 20 m/s case. Because the protuberance is interacting with fluid at warmer temperatures at a given elevation, the protuberance temperatures will also be warmer at a given elevation.

Figure 13 also shows the effect of radiation on the protuberance temperature. The predicted protuberance temperature profiles, considering the radiation into the protuberance and neglecting the radiation into the protuberance, are presented in Fig. 13. From Fig. 13, the radiation into the protuberance appears to cause only a slight change in the normalized temperatures of the protuberances. However, because the apparent enhancement is the inverse of the normalized temperature, neglecting radiation in the ES-DEM predictions significantly overestimates the enhancement, especially for the cases in which the protuberance approaches the freestream temperature. The apparent enhancement, neglecting radiation for the 20 m/s case, is 15.78. This is significantly higher than the measured apparent enhancement (8.2) and the prediction that considered radiation (10.72). For the 4.5 m/s case, neglecting radiation produces an apparent enhancement of 2.59, whereas the measured apparent enhancement and ES-DEM prediction with radiation are 2.0 and 2.36, respectively.

Although showing the trends of the apparent enhancement vs k/δ, Fig. 11 also demonstrates the effects of element thermal conductivity on the ES-DEM predictions. Because a range of thermal conductivities for plastic was found in an internet search, the ES-DEM predictions using a protuberance thermal conductivity of 0.35 W/m · K are also presented in Fig. 11. Figure 11 demonstrates that conduction along the protuberance is significant and that the apparent enhancement for a given protuberance would decrease as the thermal conductivity increased for a given value of k/δ.

The ES-DEM predictions using a protuberance thermal conductivity of 2.00 W/m · K are also provided in Fig. 11 to reinforce the effects of the protuberance thermal conductivity on the apparent enhancement. From Fig. 11, one may infer that had the investigators in Henry et al. [2] used protuberances with very high or metallic thermal conductivities, such as BBs or miniature ball bearings, they would not have measured any apparent enhancement and would have thus deduced that protuberances or isolated roughness elements do not affect the local heat transfer in laminar flow. Hence, the choice of plastic roughness elements was a fortunate one.

B. Turbulent Flow Results

Figure 14 shows the ES-DEM predictions of the apparent enhancement on the 2.8-mm-tall protuberance in turbulent flow. Figure 15 displays the apparent enhancement in turbulent flow for the 2.8 and 1.7-mm protuberances vs the Reynolds number based on the distance of the protuberance from the leading edge of the Plexiglas plate. Comparison of Fig. 14 to Fig. 3 demonstrates that the ES-DEM predictions are of the same order as the experimental measurements for the 2.8-mm-tall protuberance. As with the laminar cases, the ES-DEM predictions are larger than the experimental measurements.

Comparison of Fig. 15 to Fig. 6 shows that the ES-DEM predictions reflect the magnitudes of the apparent enhancements for both the 2.8 and 1.7-mm protuberances as functions of the Reynolds number based on the location of the protuberance from the leading edge of the plate in turbulent flow. Although the ES-DEM predictions capture the increasing apparent enhancement for the 1.7-mm protuberance, the ES-DEM does not predict the measured trend of the maximum apparent enhancement decreasing vs Re_x for the 2.8-mm protuberance.

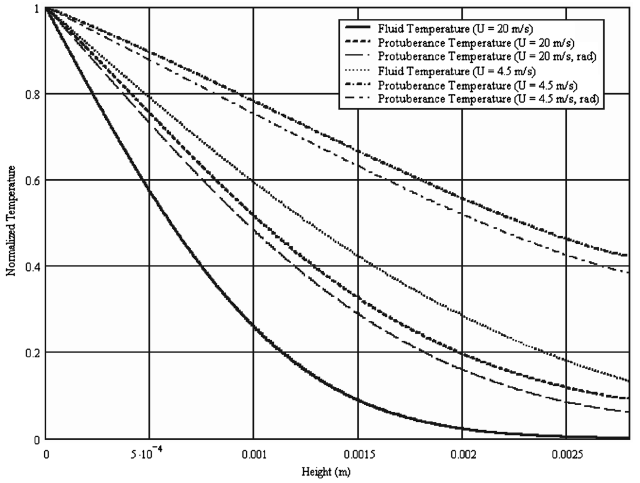

Fig. 13 The normalized fluid and protuberance temperatures for laminar flow at freestream velocities of 20 and 4.5 m/s.

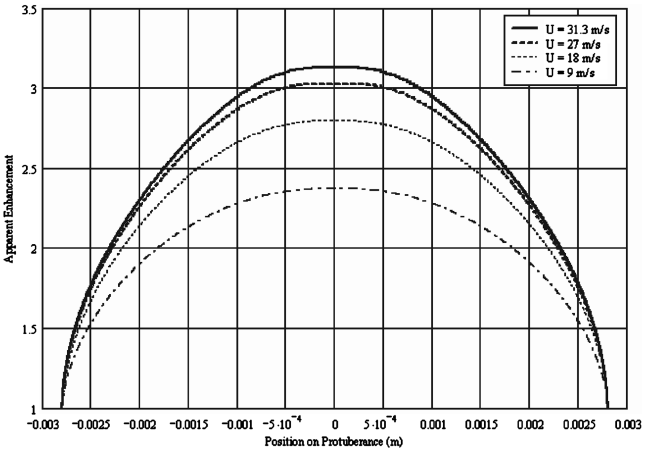

Fig. 14 Prediction of perceived heat transfer enhancement profiles on a 2.8-mm protuberance in turbulent flow as a comparison with Fig. 3.

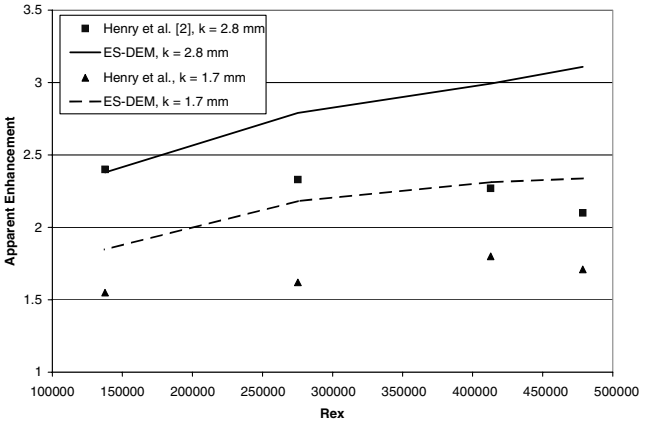

Fig. 15 Apparent heat transfer enhancement in turbulent flow vs Reynolds number for comparison with Fig. 6.

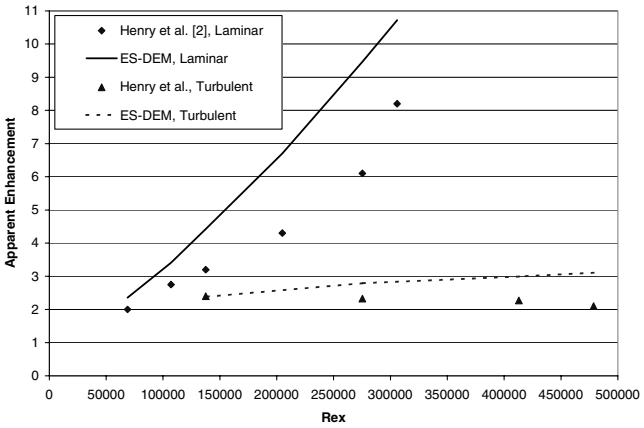

Fig. 16 The apparent enhancement for a 2.8-mm protuberance vs Reynolds number for laminar and turbulent flow.

Among the many assumptions regarding the ES-DEM analysis, the two most probable explanations for the reported decrease in apparent enhancement as the Re_x increases for the 2.8-mm protuberance are as follows:

1) Unaccounted-for secondary flow features are significantly affecting the surface temperature of the protuberance.

2) The reported decrease is due to error in the measured maximum temperature of the protuberance.

Secondary flow features are the most likely; however, the experimental uncertainty is very high. Henry et al. [2] report an estimated 20% uncertainty in the apparent enhancement for the turbulent cases. The estimate of Henry et al. only considered uncertainty from the temperature measurements and did not consider uncertainty in the spatial position of the pixel relative to the protuberance.

Although the ES-DEM did not predict the decrease in the apparent enhancement vs Re_x for the 2.8 mm protuberance, the method did capture the decrease in the apparent enhancement for the turbulent cases relative to the enhancement for the laminar cases. Figure 16 presents the apparent enhancement for the 2.8-mm protuberance in both laminar flow and turbulent flow vs Re_x. Figure 16 can be compared with Fig. 4. The ES-DEM predictions capture the relative decrease in apparent enhancement as the flow transitions after the freestream velocity is increased over 20 m/s.

Like the difference between the high-speed and low-speed laminar cases, the decrease in apparent enhancement as the flow transitions from laminar to turbulent flow is caused mainly by the temperatures of the fluid with which the protuberance is interacting. Figure 17 presents the fluid temperature and roughness element temperature for both laminar flow at 18 m/s and turbulent flow at 18 m/s for the 2.8-mm protuberance. From Fig. 17, the heated protuberance is experiencing much warmer fluid temperatures in turbulent flow than in laminar flow. The fact that the protuberance is interacting with fluid at much warmer temperatures is caused by the fact that the turbulent boundary layer is much thicker (taller) than the laminar boundary layer.

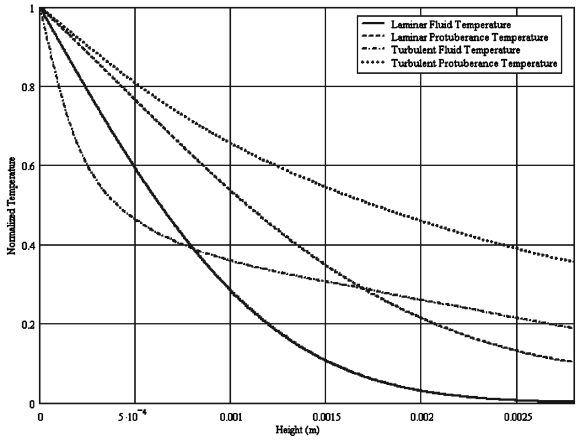

Fig. 17 The normalized fluid and protuberance temperatures for laminar and turbulent flow at 18 m/s.

V. Actual Enhancement

The ES-DEM analysis captures the trends of the apparent heat enhancement and indicates that the measurement of surface temperature on the protuberances of Henry et al. [2] cannot be used to evaluate the convective enhancement. A better measure of the enhancement of the protuberance is the *fin effectiveness* of the protuberance. The fin effectiveness of each of the protuberances used in Henry et al. cannot be determined using the experimental measurements. However, the ES-DEM predictions can be used to estimate the fin effectiveness for each experimental case of Henry et al. Because the trends of the protuberance temperature are captured by the ES-DEM method, the trends in the ES-DEM predictions of fin effectiveness should also provide some insight into the importance of the variables affecting the heat transfer enhancement of a flat wall with a protuberance.

The effectiveness of a fin is defined as the heat transferred from the extended surface over the heat transferred from a flat surface over the same planform area of the extended surface at its base. For the situations described by Henry et al. [2], the fin effectiveness is

$$\eta_e = \frac{q_{\text{fin}}}{q_{\text{flat surface}}} = \frac{-k_R A \frac{\mathrm{d}T_R}{\mathrm{d}y}\big|_{y=0}}{h_x A_0 (T_w - T_\infty)} = \frac{\int_0^k [h_d \frac{\mathrm{d}A_x}{\mathrm{d}y}(T_R - T_f) + q_r'' \frac{\mathrm{d}A_x}{\mathrm{d}y}]\,\mathrm{d}y}{h_x A_0 (T_w - T_\infty)} \tag{16}$$

When the effectiveness is placed in terms of normalized temperatures and the radiation heat transfer is evaluated as the local convection coefficient for the unperturbed flat surface, Eq. (16) becomes

$$\eta_e = \frac{-k_R \frac{\mathrm{d}\theta_R}{\mathrm{d}y}\big|_{y=0}}{h_x} = \frac{\int_0^k [h_d \frac{\mathrm{d}A_x}{\mathrm{d}y}(\theta_R - \theta_f) + h_x \frac{\mathrm{d}A_x}{\mathrm{d}y}]\,\mathrm{d}y}{h_x A_0} \tag{17}$$

Figure 18 presents the fin effectiveness of the 2.8 and 1.7-mm protuberances in laminar flow vs k/δ. Figure 18 shows that as the protuberance becomes larger than the boundary-layer thickness, the enhancement appears to approach an asymptote. The behavior of the fin effectiveness is caused by the fact that when the protuberance is as large as the thermal boundary layer, the higher elevations of the protuberance interact with fluids at the minimum possible normalized temperatures θ_f.

The fin effectiveness was also determined for each turbulent flow case provided by Henry et al. [2] for protuberance heights of 1.7 and

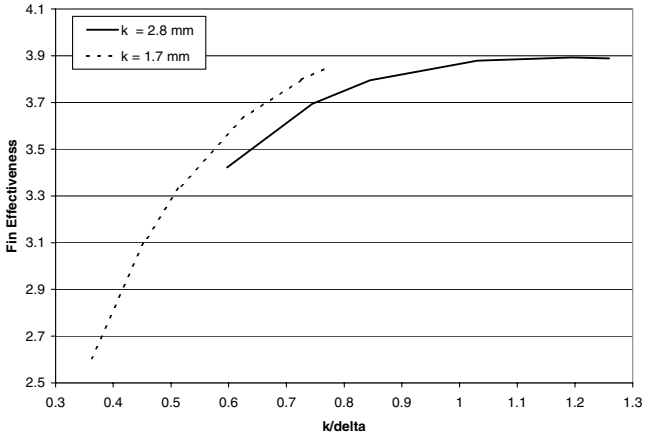

Fig. 18 Fin effectiveness vs the ratio of the protuberance height over the undisturbed laminar boundary-layer thickness.

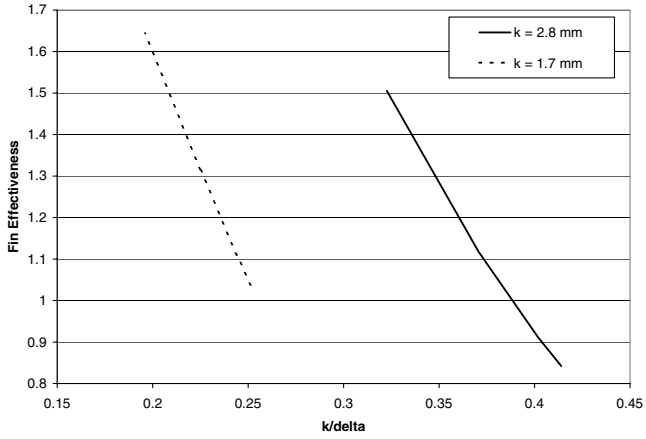

Fig. 19 Fin effectiveness vs the ratio of the protuberance height over the undisturbed turbulent boundary-layer thickness.

2.8 mm. Figure 19 displays the fin effectiveness vs k/δ for turbulent flow. Figure 19 is very interesting in that it shows that the effectiveness decreases as k/δ increases and that the effectiveness is very low. In fact, for the 2.8-mm protuberance at $k/\delta > 0.39$ (at a velocity of 31.4 m/s), the ES-DEM predicts that the protuberance is providing an insulating effect. The large drop in effectiveness from the laminar to the turbulent cases is explained by the large increase in the convection coefficient on the unperturbed surface in turbulent flow compared with laminar flow.

VI. Conclusions

The ES-DEM predictions show that the macroscale assumptions regarding radiation and conduction made to reduce the experiment's measurements of Henry et al. [2], and subsequently in Lee [3], do not hold for the microscale heat transfer occurring in the protuberances they studied. In the experiments of Henry et al., the protuberances change temperature along the height of the protuberance; thus, conduction in the protuberance cannot be neglected. The protuberances are also receiving radiation from the heat lamps; thus, although radiation from the protuberance to the ambient conditions is neglected, the radiation from the heat lamps to the protuberance cannot be neglected. Finally, and most importantly, the protuberances are interacting with fluid that is not at the freestream temperature, and because the protuberances had a low thermal conductivity, the high apparent enhancement measurements made by Henry et al. were primarily caused by the cooler fluid temperatures near the apices of the heated protuberances.

When internal conduction, radiation, and the interaction of the thermal boundary layer are considered using the ES-DEM, many of the important trends in the data of Henry et al. [2] are explained. The ES-DEM predictions capture the increasing apparent enhancement vs Re_x and k/δ. The ES-DEM captures the significant decrease in the apparent enhancement for turbulent flow vs laminar flow. The ES-DEM also indicates that the thermal conductivity of the protuberances was extremely important in determining the apparent enhancement of the protuberances.

Acknowledgments

Stephen McClain's involvement with this work was supported by the 2004 NASA Faculty Fellowship Program. All of the authors thank Tom Bond and the Icing Research Branch at NASA Glenn Research Center for support of this work.

References

[1] Vargas, M., "Current Experimental Basis for Modeling Ice Accretions on Swept Wings," AIAA Paper 2005-5188, June 2005.

[2] Henry, R. C., Hansman, R. J., Breuer, K. S., "Heat Transfer Variation on Protuberances and Surface Roughness Elements," *Journal of Thermophysics and Heat Transfer*, Vol. 9, No. 1, Mar. 1995, pp. 175–180.

[3] Lee, S., "Heat Transfer on an Airfoil with Large Distributed Leading-Edge Roughness," Master Thesis, Univ. of Illinois at Urbana–Champaign, Urbana, IL, 1997.

[4] Kerho, M. F., "Effect of Large Distributed Roughness Near an Airfoil Leading Edge on Boundary-Layer Development and Transition," Ph.D. Dissertation, Univ. of Illinois at Urbana–Champaign, Urbana, IL, 1995.

[5] Dukhan, N., "Measurement of the Convective Heat Transfer Coefficient from Ice Roughened Surfaces in Parallel and Accelerated Flows," Ph.D. Dissertation, Univ. of Toledo, Toledo, OH, Dec. 1996.

[6] Poinsatte, P. E., "Heat Transfer Measurement from a NACA 0012 Airfoil in Flight and in the NASA Lewis Icing Research Tunnel," Master Thesis, Univ. of Toledo, Toledo, OH, 1989.

[7] Kreeger, R. E., Vargas, M., McClain, S. T., "Heat Transfer over Roughness Elements Larger than the Boundary Layer," AIAA Paper 2005-5186, June 2005.

[8] Bejan, A., *Convection Heat Transfer*, 2nd ed., Wiley-Interscience, New York, 1995.

[9] Gatlin, B., and Hodge, B. K., *An Instructional Computer Program for Computing the Steady, Compressible Turbulent Flow of an Arbitrary Fluid Near a Smooth Wall*, Dept. of Mechanical Engineering, Mississippi State Univ., second printing, 1990.

[10] McClain, S. T., Hodge, B. K., and Bons, J. P., "Predicting Skin Friction and Heat Transfer for Turbulent Flow over Real Gas-Turbine Surface Roughness Using the Discrete-Element Method," *Journal of Turbomachinery*, Vol. 126, No. 2, 2004, pp. 259–267.

[11] Kreith, F., *CRC Handbook of Mechanical Engineering*, CRC Press, Boca Raton, FL, 1998.